Science of the Total Environment 506-507 (2015) 604–612

Contents lists available at ScienceDirect

Science of the Total Environment

journal homepage: www.elsevier.com/locate/scitotenv

Mapping dustfall distribution in urban areas using remote sensing and ground spectral data

Xing Yan [a,b], Wenzhong Shi [a,*], Wenji Zhao [b], Nana Luo [a,b]

[a] Department of Land Surveying and Geo-Informatics, The Hong Kong Polytechnic University, Hong Kong
[b] College of Resource Environment and Tourism, Capital Normal University, Beijing, China

HIGHLIGHTS

- A new method for dustfall mapping from satellite is proposed.
- MODIS satellite and ground based spectral data are integrated into the model.
- This method shows a good performance for dustfall detection in urban scale.

ARTICLE INFO

Article history:
Received 8 September 2014
Received in revised form 27 October 2014
Accepted 10 November 2014
Available online 26 November 2014

Editor: P. Kassomenos

Keywords:
Remote sensing
Urban areas
Dustfall
Spectral reflectance

ABSTRACT

The aim of this study was to utilize remote sensing and ground-based spectral data to assess dustfall distribution in urban areas. The ground-based spectral data denoted that dust has a significant impact on spectral features. Dusty leaves have an obviously lower reflectance than clean leaves in the near-infrared bands (780–1,300 nm). The correlation analysis between dustfall weight and spectral reflectance showed that spectroscopy in the 350–2,500-nm region produced useful dust information and could assist in dust weight estimation. A back propagation (BP) neutral network model was generated using spectral response functions and integrated remote sensing data to assess dustfall weight in the city of Beijing. Compared with actual dustfall weight, validation of the results showed a satisfactory accuracy with a lower root mean square error (RMSE) of 3.6 g/m^2. The derived dustfall distribution in Beijing indicated that dustfall was easily accumulated and increased in the south of the city. In addition, our results showed that construction sites and low-rise buildings with inappropriate land use were two main sources of dust pollution. This study offers a low-cost and effective method for investigating detailed dustfall in an urban environment. Environmental authorities may use this method for deriving dustfall distribution maps and pinpointing the sources of pollutants in urban areas.

1. Introduction

Dust diffusion and deposition are widely considered important factors affecting the ecological environment (Rashki et al., 2013). Airborne dust carrying heavy metals and particulate matter (PM) is recognized as the most harmful air component (Rai, 2013). Leaf dustfall can also impair plant growth, and a significant negative correlation was found between dust and pigment content (Prusty et al., 2005). Thus, determining the spatial distribution of dust and analyzing its sources can provide a data basis for environmental management agencies to mitigate air pollution.

However, some studies that measured atmospheric pollution by sampling particulates were expensive and time consuming (Shu et al., 2000; Likuku et al., 2013), and others required a high density of sampling points to ensure accuracy, which wasted labor and resulted in poor simultaneity (Chudnovsky and Ben-Dor, 2008). Although satellite-based solutions, which can solve problems mentioned above, have been widely applied to monitor air pollution, there are still many problems associated with this technique, such as a poor relationship between selected indices (aerosol optical thickness (AOT), etc.) and air quality (Bilal et al., 2014; Soni et al., 2014; Rahimi et al., 2014). In addition, many studies used satellite images to obtain AOT and explored its relationship with PM (Chu et al., 2003; Gupta et al., 2006; Wong et al., 2011; Luo et al., 2014). However, few researchers have applied satellite images to monitor urban dust and focused on the characteristics and source of the dustfall (Lue et al., 2010).

Recent studies revealed that dust deposited on leaf surfaces may be used as an indicator of air pollution (Yang et al., 2011; Ram et al., 2014). By collecting particulates accumulated on pine needles, Urbat et al. (2004) found that the main source of air pollution in Cologne was motor vehicles. Plant cover in urban areas could be used to acquire the

* Corresponding author at: ZS628 The Department of Land Surveying and Geo-Informatics, The Hong Kong Polytechnic University, Hung Hom, Kowloon, Hong Kong. Tel.: +852 2766 5975; fax: +852 2330 2994.
E-mail address: lswzshi@polyu.edu.hk (W. Shi).

http://dx.doi.org/10.1016/j.scitotenv.2014.11.036
0048-9697/

spatial distribution of atmospheric dust (Lu et al., 2008; Luo et al., 2013; Peng et al., 2013). Yan et al. (2014a) used the near-infrared band to estimate the amount of leaf dust deposition, and the results showed good accuracy. Chudnovsky et al. (2007) developed a new spectral-based method for estimating indoor settled dust weight. Ong et al. (2001) used visible, near-infrared, and short-wave-infrared high-resolution spectral images to quantify the leaf dust load of mangroves. Thus, remote sensing can be used to investigate dust pollution in urban areas (Zheng et al., 2001).

The purpose of this work was to establish a reliable method for monitoring dust distribution with the aid of satellite images and plant leaf spectral data. We first analyzed the correlation between spectral reflectance and dust on plants. Based on this correlation, dust distribution was obtained using a neutral network model. Finally, the sources of dust in urban areas were discussed.

2. Materials and methods

2.1. Study area

This study was conducted in the city of Beijing, which lies at east longitude 39.92° and north latitude 116.46° and covers an area of 16,807 km^2. It is located at the northern edge of the North China Plain at the junction of the Inner Mongolia Plateau, the Loess Plateau, and the North China Plain. The city's elevation decreases gradually from west to east due to the distribution of mountains and plain. The climate in Beijing is typical sub-humid warm temperature continental monsoon, with annual average temperatures between 10 °C and 12 °C and rainfall of 626 mm (Hou et al., 2012).

With the development of the city capital construction, the land cover in Beijing has changed markedly. Many main roads and residential buildings have been built to accommodate the increase in population and the consequent increase in the number of motor vehicles. Even though the Beijing city government has made great efforts to improve the environment, urban air pollution problems have become increasingly serious.

2.2. Satellite data

Moderate resolution Imaging Spectroradiometer (MODIS) Terra L1B data were obtained from NASA's Goddard Space Flight Center (http://modis.gsfc.nasa.gov). The MODIS L1B data contains calibrated and geolocated at-aperture radiances for 36 bands generated from MODIS Level 1A sensor counts (Bilal et al., 2013). This study used MODIS images acquired on July 2, August 3, and September 25 2013. Table 1 lists the weather information from the days when MODIS overpassed.

2.3. Plants collection

In this study, *Euonymus japonica* L., *Sophora japonica* L., and *Populustomentosa* L. Carr. were selected as experimental plants. *Euonymus japonica* L. is one of the main shrub species in Beijing, while *Sophora japonica* L. and *Populustomentosa* L. Carr. are also common in this area (Yang et al., 2005; Yan et al., 2014b). The above plants have been widely used for landscaping around cities. Experimental leaf samples were collected from 44 sampling locations around Beijing, and their spatial distributions are shown in Fig. 1.

Table 1
Weather information during a moderate resolution imaging spectroradiometer (MODIS) overpass.

Date	Wind direction (°)	Wind speed (m/s)	Relative humidity (%)	AOT at 550 nm
7/2/2013	290	5	49	0.11
8/3/2013	130	2	43	0.25
9/25/2013	290	4	18	0.06

2.4. Spectral measurements and processing

Initially, each plant leaf was weighed using an electronic analytic balance (1/10,000 g scale). Then, the spectral reflectances of the leaves were measured using a spectrometer (Analytical Spectral Devices FieldSpec Pro, ASD 2008) equipped with a Plant Probe (ASD auxiliary product, Halogen bulb light source type) and an ASD Leaf Clip. The ASD is a single-beam field spectroradiometer covering a range of 350–2,500 nm with a total of 2,100 spectral bands. The spectral measurements were repeated 10 times for each sample, and the mean value was taken to represent each leaf's spectral reflectance (Hansena and Schjoerring, 2003; Haboudane et al., 2004). Subsequently, leaves were cleaned with ultra-pure water and dried by absorbent paper. The cleaned leaves were reweighed, and the reflectances were measured again. Although leaf reflectance is affected by many factors, such as chlorophyll, plant health, and water content, this research compared reflectance data between dust and clean leaves, which was referred to as a samples' self-comparison and, thus, neglected possible interfering factors.

Another issue was that, due to low spatial resolution of MODIS images and the limited study area, urban cities always contained mixed pixels, which made dustfall retrieval inaccurate. Thus, when collecting leaf samples, the selected locations needed to be widely covered by vegetation cover. In addition, in order to eliminate the interference of plant type on the retrieval result, mean spectral values for three plants at single site were calculated and used for final dustfall weight calculations.

In order to transfer ground-measured data to satellite images, a leaf's narrow-band spectra was resampled at broad-band according to the relative spectral response function of MODIS (Supplementary Fig. 1). The MODIS spectral response function is as follows (Ghulam et al., 2008):

$$R_{\mathrm{MODIS}}(\lambda) = \frac{\int_{\lambda_{\min}}^{\lambda_{\max}} R_{\mathrm{Leaf}}(\lambda)\, \mathrm{f}(\lambda) d\lambda}{\int_{\lambda_{\min}}^{\lambda_{\max}} \mathrm{f}(\lambda) d\lambda} \quad (1)$$

where $R_{\mathrm{MODIS}}(\lambda)$ refers to broad-band reflectance, $f(\lambda)$ refers to the MODIS spectral response function at a corresponding waveband, $\lambda_{\min}$ and $\lambda_{\max}$ refer to the lower and upper limit of band internal, and λ indicates the center wavelength (nm) in each band. Then, the ratio of the reflectance between dust and clean leaves was calculated by the following:

$$r(\lambda) = \frac{R^{\mathrm{Dust}}_{\mathrm{MODIS}}(\lambda)}{R^{\mathrm{Clean}}_{\mathrm{MODIS}}(\lambda)} \quad (2)$$

where $R^{\mathrm{Dust}}_{\mathrm{MODIS}}(\lambda)$ and $R^{\mathrm{Clean}}_{\mathrm{MODIS}}(\lambda)$ are dust and clean leaf's reflectance corresponding to a specific band of MODIS.

2.5. Dustfall retrieval

The central idea of this retrieval method is to find out the relationship between spectral reflectance and dustfall weight and to sequentially use "dust" images and "clean" images as input parameters to calculate the whole dust distribution. Plant leaves can be cleaned by heavy continuous rain (Przybysz et al., 2014). Thus, based on Table 2, MODIS images from July 2 2013 were considered "clean" images, and images from August 3 and September 25 2013 were considered "dust" images.

The back propagation (BP) neutral network model is considered a generalization of the delta rule for nonlinear activation functions and has been successfully applied in many environmental studies (Tumbo et al., 2002; Pal et al., 2003; Sahin, 2012; Valipour et al., 2012, 2013).

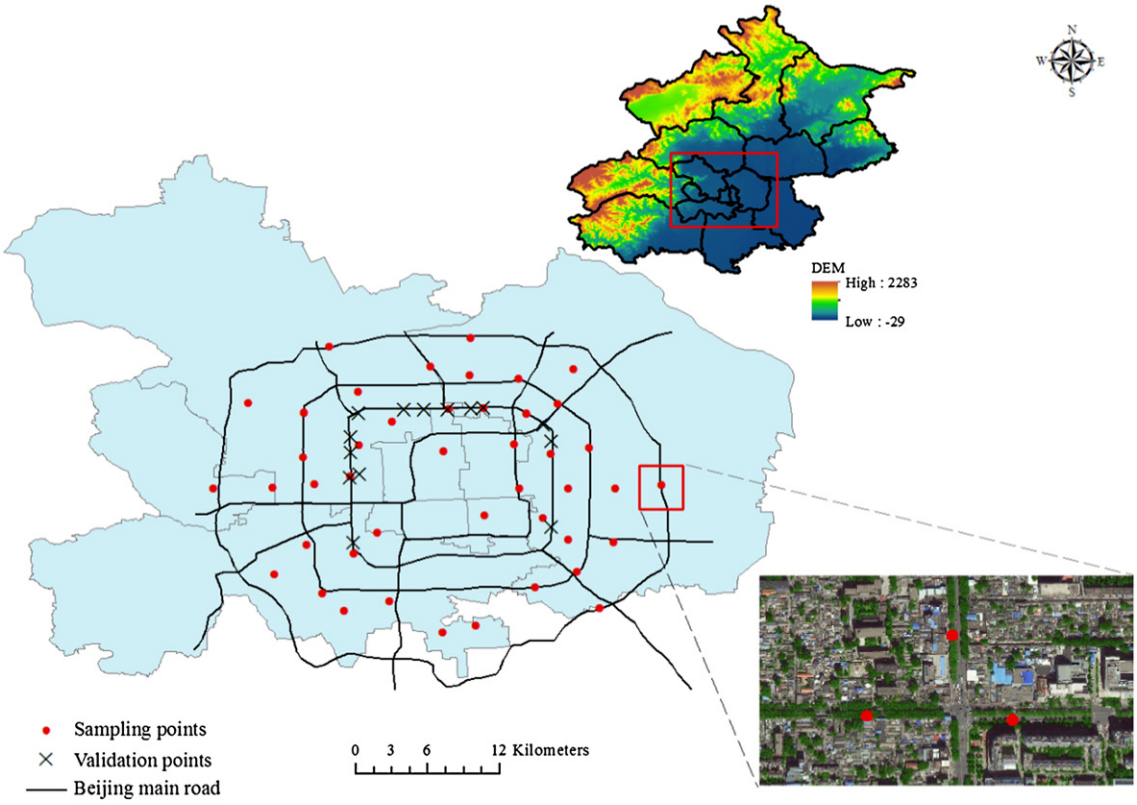

Fig. 1. Plant and validation sampling locations.

Thus, it was used to retrieval dustfall weight in this research. For our BP model, the training data were $r(\lambda)$ and dust weight per unit area (dust weight ÷ leaf area, $N = 180$), and the simulation data were MODIS reflectance ratios between dust and clean images (Fig. 2). This model consisted of 15 nodes in the middle layer; "tansig/tansig" was chosen as the transfer function and "trainlm" as the train method. These parameters were determined by optimal mean squared error (MSE) and training time epochs (Supplementary Figs. 2–4).

Fig. 3 shows the workflow for dustfall retrieval. At first, MODIS data were processed by the Second Simulation of a Satellite Signal in the Solar Spectrum (6S) model to conduct atmospheric correction and calculate surface reflectance. Then because normalized difference vegetation index (NDVI) values corresponding to sampling locations were always greater than 0.4, NDVI in these ranges were extracted. Finally, dustfall weights in these extracted regions were retrieved by a BP neutral network model, and Kriging interpolation was adopted to derive the whole dustfall distribution image.

2.6. Dustfall validation

This research used ground-measured dustfall weight to validate the retrieval results. As shown in Fig. 4, empty bottles were numbered and weighed. Then these bottles were hung on the pillars around Third Ring Road (Fig. 1) in Beijing, resulting in a total of 14 sampling sites (Hua Yuan Qiao, Li ZeQiao, Wan Shou Si, Si Tong Qiao, Ji Men Qiao, Bei Tai Ping Qiao, Ma Dian Qiao, An Zhen Qiao West, An Zhen Qiao East, San Yuan Qiao, Liang Ma Qiao, ShuangJin, Pan Jia Yuan, and Ba Yi Hu). The sampling time was from July 2 to August 1 2013.

Table 2
Weather information from June 28 to July 2, 2013.

Date	Weather condition	Air temperature (day/night)
6/28/2013	Moderate to heavy rain	33 °C/21 °C
6/29/2013	Showery rain	30 °C/22 °C
6/30/2013	Showery rain	28 °C/22 °C
7/1/2013	Heavy rain	28 °C/20 °C
7/2/2013	Sunny	34 °C/23 °C

3. Results

3.1. Influence of dustfall on plant's spectral features

Figs. 5A, B and C show the difference in spectral reflectance values between dust and clean leaves for three kinds of plants. It is apparent

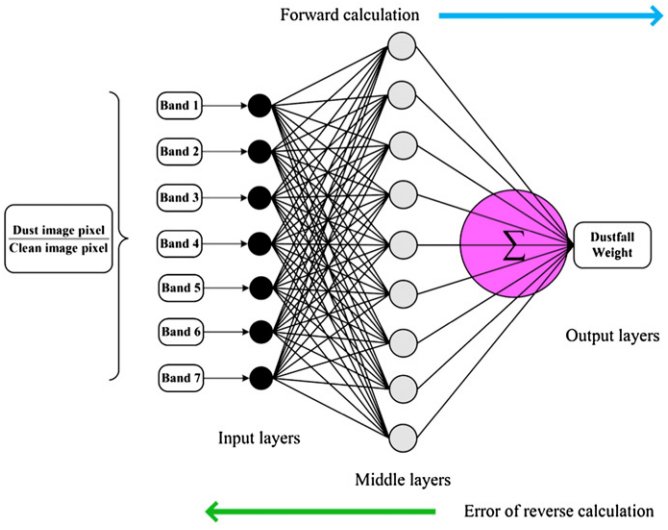

Fig. 2. Back propagation neutral network flow-chart of dustfall retrieval.

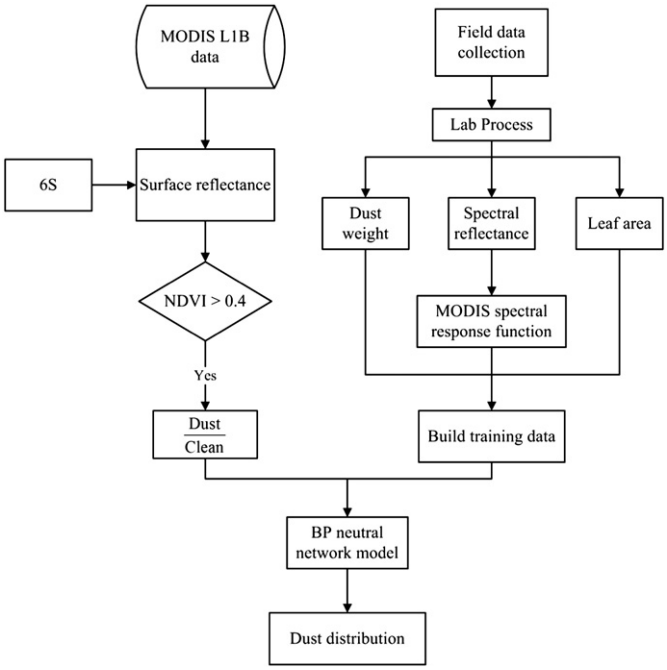

Fig. 3. Schematic diagram of dustfall retrieval.

that the trend in clean leaf reflectance is similar to dust, but their reflectances have significant differences for specific bands. Dust leaves have a higher reflectances than clean leaves at 350–700 nm, indicating that dustfall reflects energy over this interval, and at 780–1300 nm dust reflectance is obviously lower than clean leaf reflectance. Although there are fewer reflectance differences between dust and clean leaves at greater than 1300 nm, small amounts of dust sediment over this range can be effectively examined (Chudnovsky et al., 2007). These features mentioned above are consistent with previous findings by Wang et al. (2012), Luo et al. (2013), and Peng et al. (2013), which revealed that reflectance differences between dust and clean leaves indeed exist.

Fig. 5D shows the correlation coefficients between dustfall weight and leaf reflectance ratios (Dust/Clean). Generally, between 350–700 nm, 1400–1540 nm, and 1860–2500 nm, positive correlations were present with dustfall, while 700–1400 nm and 1540–1860 nm showed negative relationships. Specifically, the 750–1350 nm interval contained a low point, reaching −0.38; 1350–1550 nm and 1950–2500 nm wavebands displayed a contrary positive relationship with dust weight, and the correlation value reached 0.36.

Further correlation analysis between resampled spectral data $r(\lambda)$ and dustfall weight was performed (Fig. 6). The results showed that generally the correlation trend was consistent with Fig. 5D: r(865 nm), r(1240 nm), and r(1640 nm) were strongly and negatively related to leaf dust, peaking at −0.47, −0.48, and −0.37, respectively. In addition, r(550 nm) had the lowest positive relationship with dust (0.21). Correlation coefficients of r(470 nm), r(660 nm), and r(2130 nm) ranged from 0.3 to 0.34. Similar to our results, Chudnovsky and Ben-Dor (2008) also found that spectrum correlated with dust content. Thus, they could be used to predict the dust weight.

3.2. Dustfall retrieval and validation

Fig. 7 shows the results of dustfall retrieval in the Beijing urban area on August 3 and September 25 2013 based on BP Network. It is clear that the spatial and temporal variation of dustfall was significant during these periods. The results from August 3 reveal that high values concentrated at sampling locations in the northern corner of the city, such as Fang's Lane and An Ding Men. In addition, there were many hotspots located around the main roads with values ranging from 15 to 23 g/m^2.

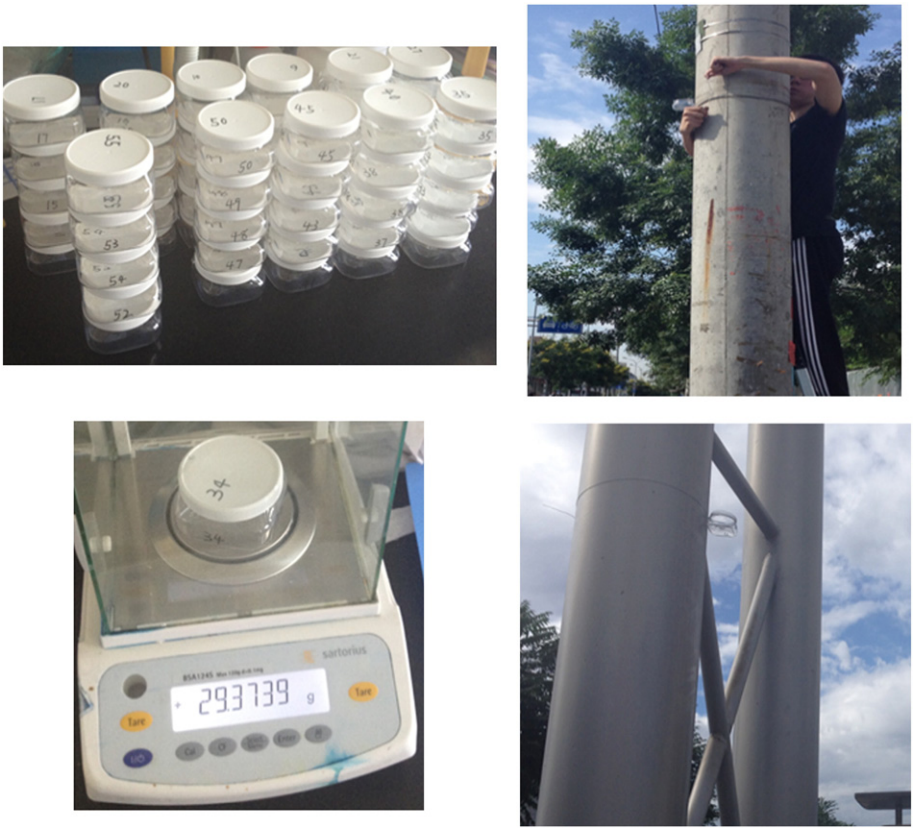

Fig. 4. Sampling bottles for validation.

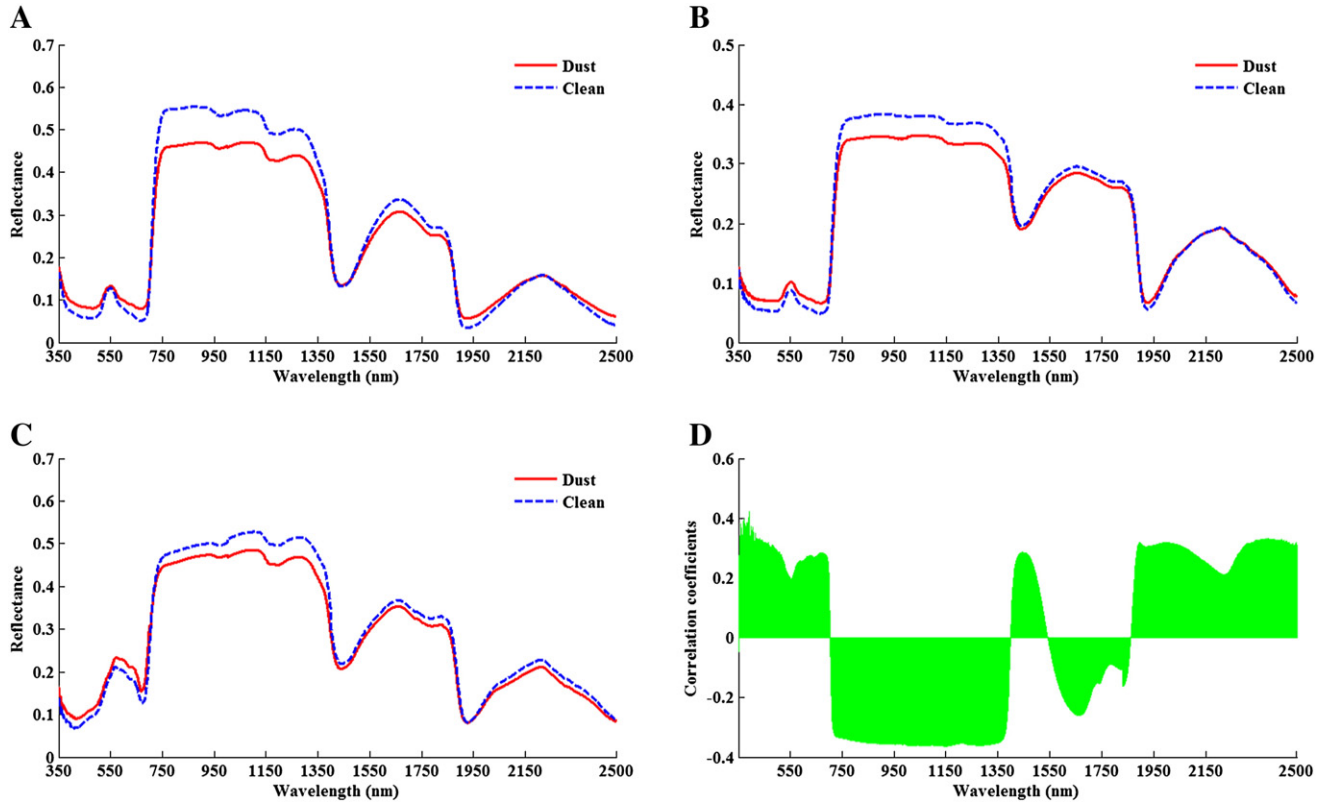

Fig. 5. Impact of dust on spectral features: (A) *Euonymus japonica*; (B) *Sophora japonica* L.; (C) *Populustomentosa* Carr.; (D) correlation analysis between reflectance ratios (Dust/Clean) of the three types of plants and dustfall weight.

On September 25, dustfall levels increased, and the hotspots continually extended. Southern areas of the city, such as the southeast of Second Ring Road and the southwest of Third Ring Road, experienced a rapid dustfall increase. To the north of the city, regions with elevated dustfall on September 25 were larger than those observed on August 3, particularly in Jian Xiang Qiao and An Hua Qiao. The dustfall histogram shown in Fig. 8 also indicates that September 25 had a mean value of 12.36 g/m^2, which was higher than the value observed on August 3 (10.98 g/m^2). Additionally, the retrieved dustfall followed normal distribution with small standard deviations of 2.104 (September 25) and 2.046 (August 3).

To evaluate the performance of the retrieval results, derived dustfall was compared with validation bottle data (Fig. 9). The comparison shows that the change trend of the retrieved results agrees well with bottle measurements, and a low root mean square error (RMSE) value

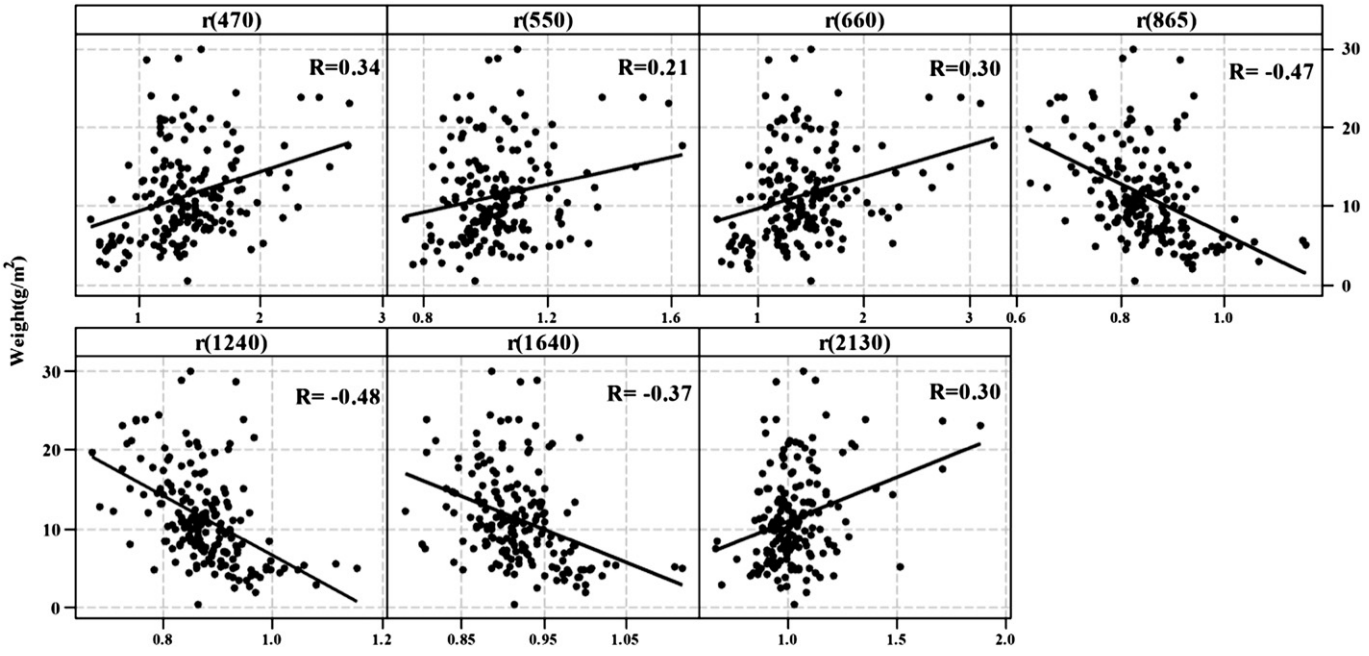

Fig. 6. Correlation analysis between $r(\lambda)$ and dustfall weight ($N = 180$).

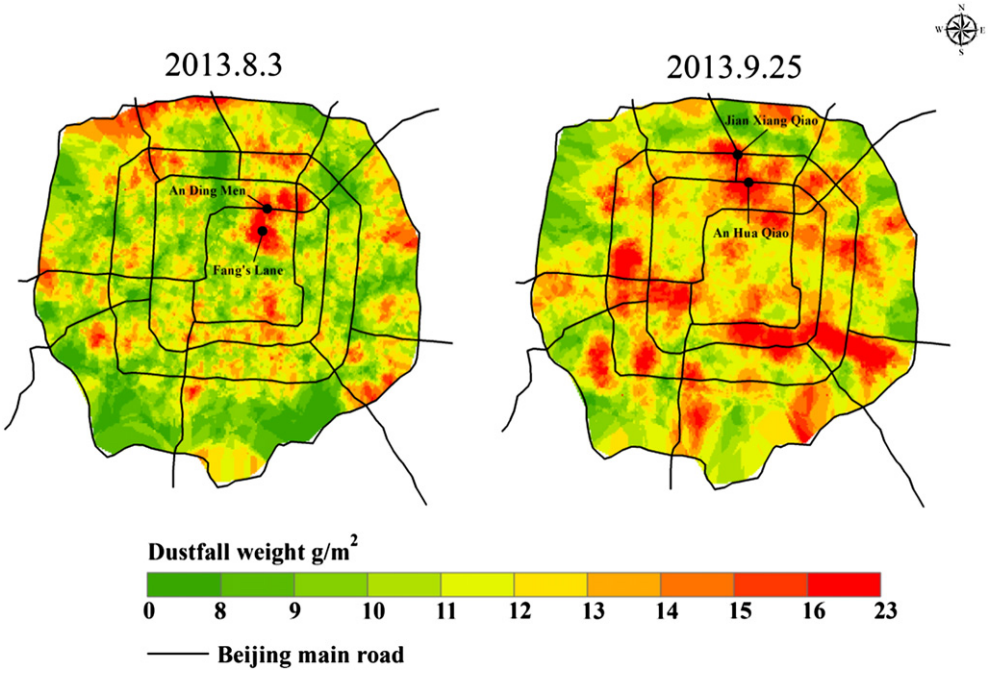

Fig. 7. Derived dustfall distribution in the city of Beijing.

of 3.6 indicates satisfactory estimation accuracy. However, the retrieved dustfall was slightly higher than the actual measurements, which may be related to the fact that satellite reflectance not only accounts for surface reflectance, but also contains noise, like bidirectional reflectance distribution function (BRDF) effects and surrounding noises. Although the 6S model was utilized to reduce these influences, there were still errors that could not be eliminated.

3.3. Dustfall source analysis

The spatial distribution of dustfall is influenced by many factors related to land cover activities, such as building and population, air flushing rates, and the distribution of transportation networks. Figs. 10A and B show an under-construction subway station beside the Olympic Sports Center and a construction site for business activities, respectively. These construction projects are all in the high dustfall level regions and could be the main source of dust pollution (Tsang, 1996). Wen and Yang (2006) also indicated that construction sites contributed dust and particles and were prone to causing air pollution problems.

Due to the old age of Beijing, some of the buildings in the studied area are low rise and in dilapidated condition (Fig. 10C). They are closely packed along the road with little space between buildings (Fig. 11). The lack of space between the buildings can easily trap air emissions, and dustfall would be serious in these air sheds with limited dispersive capacity. Homeowners might want to maximize the use of land, resulting in limited open spaces, which are necessary for air ventilation.

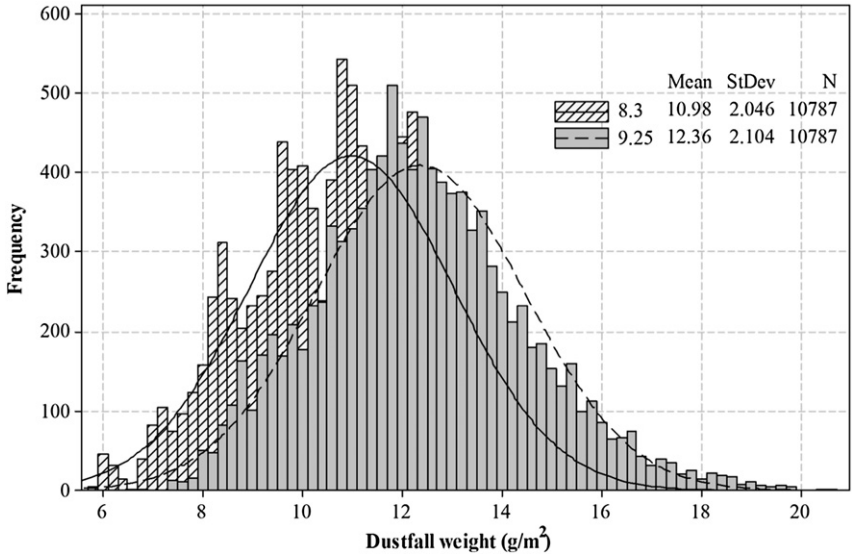

Fig. 8. Histogram of derived dustfall on August 3 and September 25, 2013.

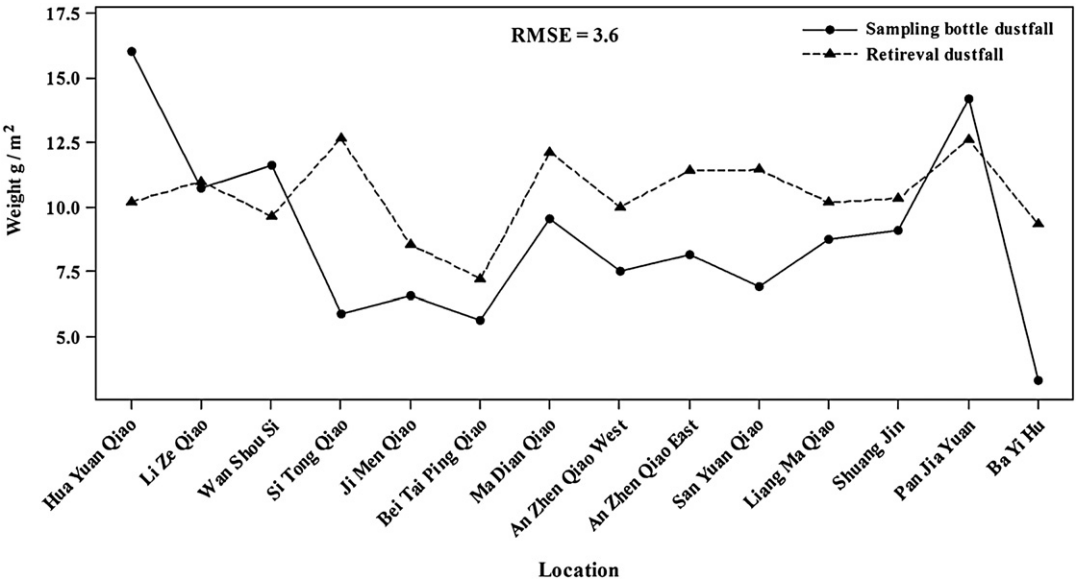

Fig. 9. Retrieved dustfall validation with actual measurement data.

In addition, transport related dust pollution could also be serious in these areas. Emissions from vehicles diffuse poorly due to the lack of space between old buildings.

4. Discussion

Combined with ground sampling and spectrum measurement data, satellite can be used as a tool to map dustfall distribution over large areas. The method proposed in this research not only represents an original technique to observe air pollution by calculating the whole dust distribution but also directly connects satellite data to observed values at a very low cost. Unfortunately, the low spatial resolution of MODIS cannot exactly match the sampling sites for leaf collection and, thus, a high accuracy retrieval result is not expected. To combat this limitation, this study selected sampling locations that were widely covered by vegetation and corresponded to satellite pixels as much as possible to

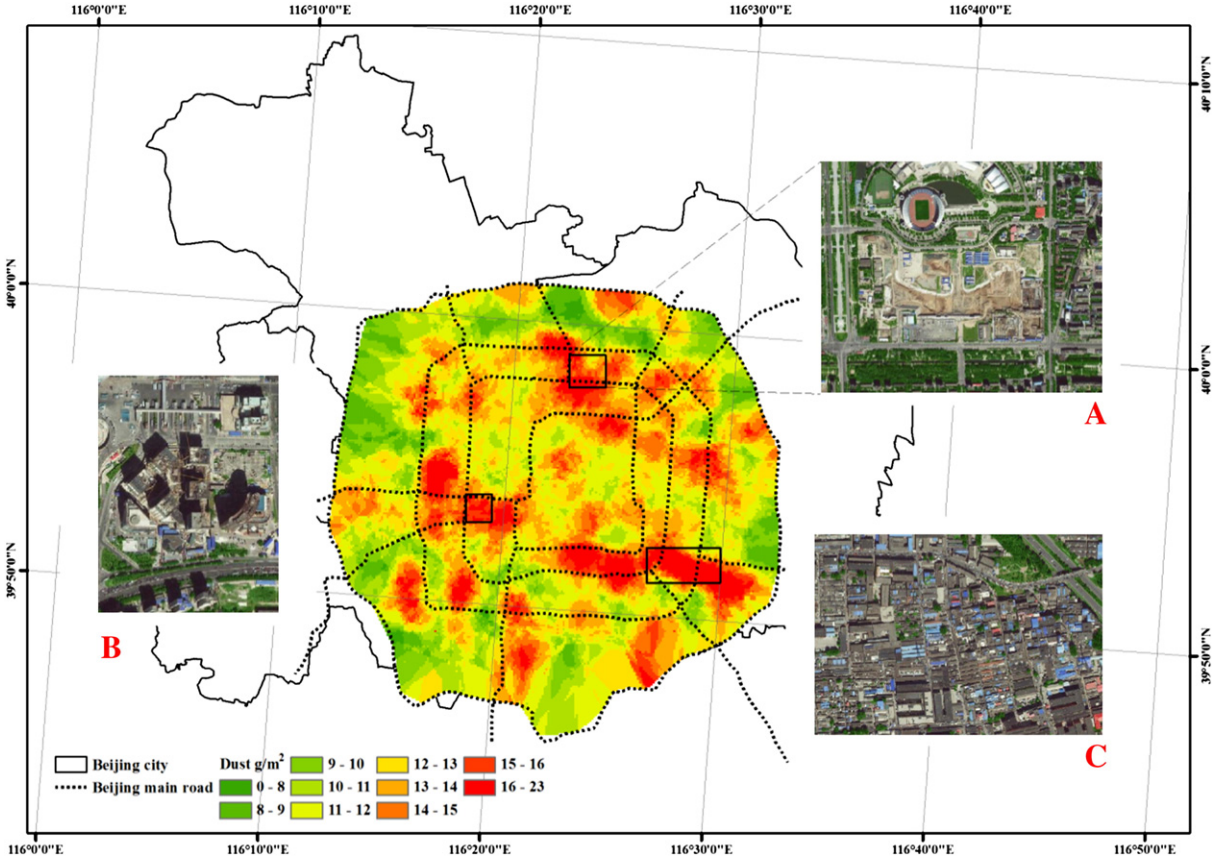

Fig. 10. Analysis of dustfall source: (A) an under-construction subway station; (B) a downtown business construction site; (C) cottage areas.

Fig. 11. Buildings in cottage areas.

reduce the influence of mixed pixels. Another issue of concern is that leaf reflectance can be altered by vegetation phenology. Liang et al. (2006) indicated that, except for extreme weather impacts, surface properties do not change dramatically within a 3-month period. From the validation results, the trend of retrieved dustfall agrees well with real measurements, which illuminates the reliability of this method and demonstrates the utility of the results as a tool for curbing environmental pollution. Nevertheless, there are still errors between satellite and ground based data, and the retrieved results do not have a very high accuracy. Thus, techniques for further improving accuracy remain vital and require further study.

5. Conclusions

This study aimed at obtaining dustfall distribution on a city-scale using satellite images and ground-measured leaf dustfall. Dustfall has a significant impact on leaf spectral features, especially in the near-infrared band (780–1300 nm), where dusty leaves have lower reflectance values than clean leaves. Specifically, $r(865)$ and $r(1240)$ are most closely related to dustfall, with the correlation coefficients reaching −0.48 and −0.47, respectively.

Through a BP neural network model, Beijing city's dustfall distribution was estimated. The results revealed that dustfall easily accumulated and increased in the south of the city. The concentrations of dustfall in the city conformed more to the circular zonation pattern. The validation of the results showed a satisfactory performance compared with the actual sampling bottles' dustfall weight (RMSE = 3.6). Using dustfall images, two main sources of dustfall were found: construction sites and low-rise building with old and inappropriate land use, which corroborates earlier observations (Tsang, 1996; Wen and Yang, 2006).

This study illustrates that using remote sensing to detect dustfall can be an effective and appropriate method of monitoring air pollution levels. In addition, it provides an alternative solution for environmental authorities to analyze dust sources more efficiently and economically. Most importantly, our method can be further modified and applied to other satellite images (e.g., Landsat).

Acknowledgements

The work presented in this paper is supported by the Ministry of Science and Technology of China (Project Nos. 2012BAJ15B04, 2012AA12A305) and the Hong Kong Polytechnic University (Project Nos. 1-ZV4 F, G-U753, G-YK75, G-YJ75). The authors wish to acknowledge the NASA Goddard Earth Science Distributed Active Archive Center for the MODIS data.

Appendix A. Supplementary data

Supplementary data to this article can be found online at http://dx.doi.org/10.1016/j.scitotenv.2014.11.036.

References

Bilal M, Nichol JE, Bleiweiss MP, Dubois D. A Simplified high resolution MODIS Aerosol Retrieval Algorithm (SARA) for use over mixed surfaces. Remote Sens Environ 2013;136:135–45.
Bilal M, Nichol JE, Chan PW. Validation and accuracy assessment of a Simplified Aerosol Retrieval Algorithm (SARA) over Beijing under low and high aerosol loadings and dust storms. Remote Sens Environ 2014;153:50–60.
Chu DA, Kaufman YJ, Zibordi G, Chern JD, Mao J, Li C, et al. Global monitoring of air pollution over land from the Earth observing System-Terra Moderate Resolution Imaging Spectroradiometer (MODIS). J Geophys Res 2003;108:D21.
Chudnovsky A, Ben-Dor E. Application of visible-, near-infrared, and short-wave infrared (400–2500 nm) reflectance spectroscopy in quantitatively assessing settled dust in the indoor environment. Case study in dwellings and office environments. Sci Total Environ 2008;393:198–213.
Chudnovsky A, Ben-Dor E, Saaroin H. Reflectance spectroscopy of indoor settled dust in Tel Aviv, Israel; comparison between the spring and the summer seasons. Adv Geosci 2007;1:51–7.
Ghulam A, Li ZL, Qin Q, Yimit H, Wang J. Estimating crop water stress with ETM + NIR and SWIR data. Agric For Meteorol 2008;148:1679–95.
Gupta P, Christopher SA, Wang J, Gehrig R, Lee Y, Kumar N. Satellite remote sensing of particulate matter and air quality assessment over global cities. Atmos Environ 2006;40:5880–92.
Haboudane D, Miller JR, Pattery E, Zarco-Tejad PJ, Strachan IB. Hyperspectral vegetation indices and novel algorithms for predicting green LAI of crop canopies: modeling and validation in the context of precision agriculture. Remote Sens Environ 2004;90:337–52.
Hansena PM, Schjoerring JK. Reflectance measurement of canopy biomass and nitrogen status in wheat crops using normalized difference vegetation indices and partial least squares regression. Remote Sens Environ 2003;86:542–53.
Hou P, Jiang WG, Cao GZ, Li J. Aerosol retrieval with satellite image and correlation analyses between aerosol distribution and urban under laying surface. Agric For Meteorol 2012;33:3232–51.
Liang SL, Zhong B, Fang HL. Improved estimation of aerosol optical depth from MODIS imagery over land surfaces. Remote Sens Environ 2006;104:416–25.
Likuku AS, Gaboutloeloe GK, Mmolawa KB. Determination and source apportionment of selected heavy metals in aerosol samples collected from Sebele. Am J Environ Sci 2013;9:188–200.
Lu SG, Zheng YW, Bai SQ. A HRTEM/EDX approach to identification of the source of dust particles on urban tree leaves. Atmos Environ 2008;42:6431–41.
Lue YL, Liu LY, Hu X, Wang L, Guo LL, Gao SY, et al. Characteristics and provenance of dustfall during an unusual floating dust event. Atmos Environ 2010;44:3477–84.
Luo NN, Zhao WJ, Yan X. Study on inversion of dust-fall on plant leaves based on high spectral data. Spectrosc Spectr Anal 2013;33:2715–20.
Luo NN, Zhao WJ, Yan X. Integrated aerosol optical thickness, gaseous pollutants and meteorological parameters to estimate ground PM2.5 concentration. Fresenius Environ Bull 2014;23:2567–77.
Ong C, Cudahy T, Caccetta M, Hick P, Piggott M. Quantifying dust loading on mangroves using hyperspectral techniques. Geosci Remote Sens Lett 2001;1:296–8.
Pal NR, Pal S, Das J, Majumdar K. SOFM-MLP: a hybrid neural network for atmospheric temperature prediction. IEEE Geosci Remote Sens Lett 2003;41:2783–91.
Peng J, Xiang HY, Wang JQ, Ji WJ, Liu WY, Chi CM, et al. Quantitative model of foliar dustfall content using hyperspectral remote sensing. J Infrared Millim Waves 2013;32:313–8.

Prusty BAK, Mishra PC, Azeez PA. Dust accumulation and leaf pigment content in vegetation near the national high way at Sambalpur, Orissa, India. Ecotoxicol Environ Saf 2005;60:228–35.
Przybysz A, Saebo A, Hanslin HM, Gawronski SW. Accumulation of particulate matter and trace elements on vegetation as affected by pollution level, rainfall and the passage of time. Sci Total Environ 2014;481:360–9.
Rahimi S, Sefidkouhi MAG, Raeini-Sarjaz M, Valipour M. Estimation of actual evapotranspiration by using MODIS images (a case study: Tajan catchment). Arch Agron Soil Sci 2014. http://dx.doi.org/10.1080/03650340.2014.944904.
Rai PK. Environmental magnetic studies of particulates with special reference to biomagnetic monitoring using roadside plant leaves. Atmos Environ 2013;72:113–29.
Ram SS, Kumar RV, Chaudhuri P, Chanda S, Santra SC, Sudarshan M, et al. Physico-chemical characterization of street dust and re-suspended dust on plant canopies: An approach for finger printing the urban environment. Ecol Indic 2014;36:334–8.
Rashki A, Eriksson PG, Rautenbach CJW, Kaskaoutis DG, Grote W, Dykstra J. Assessment of chemical and mineralogical characteristics of airborne dust in the Sistan region, Iran. Chemosphere 2013;90:227–36.
Sahin M. Modelling of air temperature using remote sensing and artificial neural network in Turkey. Adv Space Res 2012;50:973–85.
Shu J, Dearing JA, Morse AP, Lizhong Y, Yuan N. Determining the sources of atmospheric particles in Shanghai, China, from magnetic and geochemical properties. Atmos Environ 2000;35:2615–25.
Soni K, Kapoor S, Parmar KS, Kaskaoutis DG. Statistical analysis of aerosols over the Gangetic–Himalayan region using ARIMA model based on long-term MODIS observations. Atom Res 2014;149:174–92.
Tsang FY. To improve air quality through land use planning a case study in western district [Master Dissertation] University of Hong Kong; 1996.
Tumbo SD, Wagner DG, Heinemann PH. Hyper spectral-based neural network for predicting chlorophyll status in corn. Trans ASAE 2002;45:825–32.
Urbat M, Lehndorff E, Schwark L. Biomonitoring of air quality in the Cologne conurbation using pine needles as a passive sampler-Part I: magnetic properties. Atmos Environ 2004;38:3781–92.
Valipour M, Banihabib ME, Behbahani SMR. Monthly inflow forecasting using autoregressive artificial neural network. J Appl Sci 2012;12:2139–47.
Valipour M, Banihabib ME, Behbahani SMR. Comparison of the ARMA, ARIMA, and the autoregressive artificial neural network models in forecasting the monthly inflow of Dez dam reservoir. J Hydrol 2013;476:433–41.
Wang T, Liu Y, Wu HY, Zuo YM. Influence of foliar dust on crop reflectance spectrum and nitrogen monitoring. Spectrosc Spectr Anal 2012;32:1895–8.
Wen QH, Yang SH. Urban air pollution patterns, land use, and thermal landscape: an examination of the linkage using GIS. Environ Monit Assess 2006;117:463–89.
Wong MS, Nichol JE, Lee KH. An operational MODIS aerosol retrieval algorithm at high spatial resolution, and its application over a complex urban region. Atmos Res 2011;99:579–89.
Yan X, Shi WZ, Zhao WJ, Luo NN. Estimation of atmospheric dust on plant leaves based on spectral features. Spectrosc Lett 2014a;47:536–42.
Yan X, Shi WZ, Zhao WJ, Luo NN. Impact of aerosols and atmospheric particles on plant leaf proteins. Atmos Environ 2014b;88:115–22.
Yang J, McBride J, Zhou JX, Sun ZY. The urban forest in Beijing and its role in air pollution reduction. Urban For Urban Green 2005;3:65–78.
Yang T, Zeng Q, Liu Z, Liu Q. Magnetic properties of the road dusts from two parks in Wuhan city, China: implications for mapping urban environment. Environ Monit Assess 2011;177:637–48.
Zheng XJ, Lu WJ, Luo JN. Research on the dust storm monitoring using multi-channel meteorological satellite data. J Remote Sens 2001;5:301–5.